Title

Unseeded, spontaneous nucleation of spherulitic magnesium calcite

Authors

Prus, Marzena

Li, Chunhui

Kędra-Królik, Karolina

et al.

Publication Date

2021-07-01

DOI

10.1016/j.jcis.2021.03.002

Peer reviewed

Unseeded, spontaneous nucleation of spherulitic magnesium calcite

Marzena Prus,[1*] Chunhui Li,[2] Karolina Kędra-Królik,[1] Wojciech Piasecki,[3] Karolina Lament,[4] Tajana Begović,[5] Piotr Zarzycki,[1,2*]

[1]*Institute of Physical Chemistry, Polish Academy of Sciences, Warsaw, Poland*
[2]*Energy Geosciences Division, Lawrence Berkeley National Laboratory, 1 Cyclotron Road, Berkeley, California, United States*[3]*Faculty of Physical*
[3]*Education and Health, Józef Piłsudski University of Physical Education in Warsaw, Biala Podlaska, Poland*
[4]*Regional Research and Development Center, Józef Piłsudski University of Physical Education in Warsaw, Biala Podlaska, Poland*
[5]*Department of Chemistry, Faculty of Science, University of Zagreb, Zagreb, Croatia*

Abstract

Most of the sedimentary carbonates deposited in the marine environments are composed of calcium carbonate minerals with varying amounts of incorporated Mg^{2+}. However, understanding how interactions of impurities with carbonate and their incorporation affect sediments behavior remains a challenge. Here, a new insight is obtained by monitoring solution composition, morphology, and electrokinetic potential of carbonate particles formed in a spontaneous unseeded batch precipitation experiment using electrochemical and scanning electron microscopy methods. The solid composition and growth rate are extracted from changes in the bulk composition and fitted to chemical affinity rate law, revealing that the precipitation pathway consists of second-order dissolution and first-order precipitation. The molecular dynamics simulations show that the lattice strain induced by randomly substituting Ca^{2+} by Mg^{2+} stabilizes spherical nanoparticles and reduces their surface area and volume.

Combining kinetics and thermodynamics insight, we conclude that variation in the carbonate bulk and interfacial energies, along with the solution supersaturation, lead to the dissolution-precipitation transformation pathway from Mg-rich to Mg-poor carbonate phase that preserves spherulitic morphology. Our findings are relevant for long-standing questions of how impurities influence diagenesis of carbonate sediments and spherulitic carbonate particles' origin.

Keywords: magnesium calcite, spherulites, molecular simulations, solid transformation, precipitation-dissolution, growth rate

1. Introduction

The inorganic and organic compounds abundant in the marine environment are believed to regulate bicarbonate minerals formation and morphologies [1-4]. Calcite precipitated in seawater always contains Mg^{2+} [5]. However, our knowledge of how Mg^{2+} influences carbonate precipitation pathways remains limited despite decades of studies [1, 6-18]. A major challenge is to gain direct experimental insight into nucleation, transformation, and growth of carbonates in the environmental conditions and then extract the mechanism governing each of these steps.

Carbonate nucleation and growth pathways are complex and often consist of multiple steps and competitive routes, even in the absence of an impurity [4, 11, 12, 19-32]. Much more complex reaction patterns should emerge if impurities are considered. It is generally accepted that calcium carbonate coprecipitating with magnesium carbonate forms more soluble carbonate phases than pure calcite for several reasons [1, 6-10, 33]. Firstly, the Mg^{2+} ions are smaller than Ca^{2+} and generate defects (misfits, dislocations) and lattice strain within precipitate that destabilize solid structure and lead to increased solubility and reduced solution supersaturation [1, 33]. However, in some cases, Mg-rich nanoprecipitates' alignment results in strengthening and toughening the bio-carbonate matrix [34-36]. Secondly, because the Mg^{2+} ions bind water more strongly than Ca^{2+}, they introduce their hydration water into the sediment and, as a result, delay transformations to more stable and usually dehydrated carbonate polymorphs [1, 6-10, 33]. Finally, the ion-pairing between carbonate and magnesium lowers solution supersaturation by decreasing the number of carbonate ions available for solid growth [10, 37].

* Corresponding author. Tel.: +1-510-486-6272; fax: +1-510-486-6455.
E-mail address: ppzarzycki@lbl.gov (PZ) or mprus@ichf.edu.pl (MP)

These processes underpin an increased solubility of a precipitate, enhanced stability of metastable amorphous/polymorphs phases, and significantly reduced precipitation rate [1, 11-18].

A fascinating aspect of the carbonate (bio)minerals is a wide variety of observed morphologies [38-41]. The spherulitic shape is especially intriguing as it is not generally expected for inorganic crystals. The spherulitic carbonates are abundant in lacustrine, hyper alkaline, and saline environments [42]; however, it is still debated what triggers spherulitic growth. Recently, Tsao et al. [43] showed that the presence of Mg^{2+} ions is the most decisive factor in the formation of spherulites. It has also been demonstrated that environmentally-common organic acids or polysaccharides facilitate spherulitic growth (e.g., bacterial outer membrane) [42, 44, 45].

Regarding the mechanism, it has been proposed that phase separation within the precipitate into Mg-depleted core, and Mg-rich shell or domains, and subsequent growth of the spherulitic crystalline core within the amorphous shell are all contributing factors [43, 45-47]. Liu et al. [3] showed that because Mg^{2+} ions bring their hydration water into the amorphous phase, a direct spherulitic shape-preserving transformation into Mg-calcite omitting the dissolution-precipitation pathway is possible. The water molecules introduced by incorporating hydrated Mg^{2+} provide the conformational space required for ion rearrangement leading to calcite formation within the spherulitic intermediate phase [3].

Prus et al. [48] showed that the transformation of vaterite to calcite in an unseeded spontaneous precipitation experiment could be studied by monitoring solution composition and electrokinetic potential [48]. Here, by using a similar experimental approach, we try to answer the question of how growth rate and solid composition are changing along the magnesian calcite nucleation, growth, and transformation pathways. We also ask whether morphology or the intermediate phases can be preserved by carbonate precipitation from the Mg^{2+}-rich solution – as recently suggested by others [3, 43]. The molecular dynamics simulations and X-ray diffraction are used to get a structural and energetic insight into Mg^{2+}-substituted calcites, particularly the variation of the spherulitic interfacial energies particle with its composition.

Materials and methods

1.1. Reagents and materials and experimental protocol

Reagents ($CaCl_2$, Na_2CO_3, $MgCl_2$, NaCl) of analytical grade were obtained from Sigma-Aldrich and Chempur. We used deionized, distilled water (Milli-Q-PLUS 185 System) to prepare three identical solutions containing 2 mM $CaCl_2$ + 2 mM Na_2CO_3 solutions + 100 mM NaCl solutions. We added $MgCl_2$ to two solutions to have its concentration equal to 1 mM and 2 mM, respectively. The solutions were prepared in an electrochemical cell, filled with argon gas. The concentration of free calcium ions in the solution and the bulk pH value were measured using a calcium-selective polymer membrane electrode (Metrohm, 6.0508.110, reproducibility ±4%, pH range 2–12, detection limit 5×10^{-4} mM Ca^{2+}) and a combined pH-glass electrode (Metrohm, 6.0258.000). The electrokinetic potential was measured using Zetasizer Nano ZS (Malvern), with a light absorbance at λ=632.8 nm, laser incidence at 171º. All measurements were carried at room temperature, starting one minute after the reagents are mixed and sealed. Each measurement was repeated at least three times, and the average data are reported here. SEM images of carbonate precipitates were taken three hours after the reagents had been mixed using FEI Nova NanoSEM 450 with an accelerating voltage of 2 kV. A more detailed discussion about the experimental protocol can be found elsewhere [48]. The crystal structure of carbonate precipitates was characterized by Bruker D8 Advance X-ray diffractometer equipped with Cu Kα (l=0.154 nm) lamp and Lynx Eye Array detector. The spectra were collected in the reflexive mode with a scan speed equal 0.02^{o} sec^{-1}.

1.2. Extracting growth rate and stoichiometry from changes in bulk composition

The magnesian calcite precipitation can be described by the following chemical reaction [5]:

$$(1-x)\mathrm{Ca}^{2+} + x\mathrm{Mg}^{2+} + \mathrm{CO}_3^{2-} \longrightarrow \mathrm{Ca}_{1-x}\mathrm{Mg}_x\mathrm{CO}_3 \quad (1)$$

where x stands for a fraction of Ca^{2+} replaced by Mg^{2+} in the solid phase. The thermodynamic equilibrium constant for precipitation can be expressed in terms of the solubility product K_{sp} ($K_{precipitation} = 1/K_{sp}$):

$$K_{sp} = \{\mathrm{Ca}^{2+}\}^{1-x}\{\mathrm{Mg}^{2+}\}^{x}\{\mathrm{CO}_3^{2-}\} = (\gamma_{\mathrm{Ca}}[\mathrm{Ca}^{2+}])^{1-x}(\gamma_{\mathrm{Mg}}[\mathrm{Mg}^{2+}])^{x}(\gamma_{\mathrm{CO_3}}[\mathrm{CO}_3^{2-}]) \quad (2)$$

where γ_i are activity coefficients of *i*-ion in the solution and [5], and square and curly brackets indicate ion concentration and activity in the solution, respectively. As shown by Mucci et al. [7-10], the Mg/Ca ratio in the solid is linearly correlated to Mg/Ca ratio in solution. What is more, Mucci et al. [7-10] found that there is a unique incorporation ratio *x* for a given Mg/Ca ratio in the solution in the case of the calcite precipitating from seawater.

The growth rate is often estimated by monitoring temporal changes in free calcium ion concentration in the bulk solution [49-51]. In the absence of Mg^{2+}, the rate of changes in bulk Ca^{2+} concentration is related to a precipitation/growth rate, that is $R_g = -\frac{d[\mathrm{Ca}^{2+}]}{\mathrm{dt}}$.

The solid composition (x in $\mathrm{Ca}_{1-x}\mathrm{Mg}_x\mathrm{CO}_3$) at any given moment of time *t* can be estimated from an excess of free calcium ions concentration in bulk as compared with precipitation from the Mg-free solution:

$$x(t) = \frac{[\mathrm{Ca}^{2+}]_{\mathrm{solid}}^{\mathrm{Mg2+=0}} - [\mathrm{Ca}^{2+}]_{\mathrm{solid}}^{\mathrm{Mg2+}}}{[\mathrm{Ca}^{2+}]_{\mathrm{solid}}^{\mathrm{Mg2+=0}}} = \frac{[\mathrm{Ca}^{2+}]_{\mathrm{liquid}}^{\mathrm{Mg2+}} - [\mathrm{Ca}^{2+}]_{\mathrm{liquid}}^{\mathrm{Mg2+=0}}}{[\mathrm{Ca}^{2+}(t=0)]_{\mathrm{liquid}} - [\mathrm{Ca}^{2+}]_{\mathrm{liquid}}^{\mathrm{Mg2+=0}}} \quad (3)$$

where concentrations, denoted by square brackets, vary in time and $[\mathrm{Ca}^{2+}(t=0)]_{\mathrm{liquid}}$ corresponds to the initial Ca^{2+} concentration.

One of the most convenient ways to express solid enrichment in coprecipitating ion is to calculate the ratio of solid enrichment relative to the bulk solution depletion. This quantity is called the Henderson-Kracek distribution coefficient, and it is defined as [52]:

$$D = \frac{\left(\frac{[\mathrm{Mg}^{2+}]}{[\mathrm{Ca}^{2+}]}\right)_{\mathrm{solid}}}{\left(\frac{[\mathrm{Mg}^{2+}]}{[\mathrm{Ca}^{2+}]}\right)_{\mathrm{liquid}}} \quad (4)$$

D value close to 0 indicates lack of Mg^{2+} coprecipitation; a value approaching infinity suggests complete depletion of Mg^{2+} in the solution, whereas *D* equals one means that there is an equal partitioning of Ca^{2+} and Mg^{2+} and we cannot separate these ions through selective precipitation [52].

1.3. Modeling growth rate

As a solid phase emerges from a supersaturated solution, the concentration of the solid-constituting ions diminishes. As a result, the driving force for precipitation decreases, and the system approaches equilibrium. In equilibrium, the ion activity product is equal to the solubility product. Because the driving force for growth is the free energy difference between ions in the solid and in the solution (ΔG), the growth rate is often expressed as a function of disequilibrium. Such models are referred to as the chemical affinity-based rate laws [6, 49, 50, 53]. In general, the growth rate, R_g, is given by [54-57]:

$$R_g = k\left(\exp\left[n\frac{\Delta G}{RT}\right] - 1\right)^m \quad (5)$$

where *k* is a rate constant, R is the gas constant, T is the absolute temperature, *n,m* are coefficients describing the strength of the relationship between rate and driving force [58-60]; ΔG is the free energy difference (or disequilibrium) that is defined by the solution supersaturation (Ω) or saturation index (SI) as follows:

$$\Delta G = RT \ln \Omega, \quad \Omega = \frac{\{Ca^{2+}\}\{CO_3^{-2}\}}{K_{sp(calcite)}}, \quad SI = \log_{10} \Omega \tag{6}$$

where $\{Ca^{2+}\}, \{CO_3^{-2}\}$ are activities of solid-forming constituting ions, $K_{sp(calcite)}$ is the mineral solubility product, which is defined as the ion activity product in the solution at equilibrium.

The affinity-based rate law does not explicitly express rate as a function of time, the time is introduced implicitly through a time-dependence of the free energy difference ΔG(t) or supersaturation Ω(t). To apply these rate laws in our measurements, we express saturation as a time-dependent function of free calcium activity in bulk.

1.4. Molecular Dynamics Simulations

In order to gain a molecular-level insight into the role of Mg^{2+} substitutions in stabilizing spherulitic morphologies of magnesium carbonate, we carry out a sequence of molecular dynamics simulations of the spherical particle in a vacuum and immersed in bulk water, as well as the periodic bulk carbonate phase varying amount of Mg^{2+} substitutions from x = 0 to x = 0.7 in $Ca_{1-x}Mg_xCO_3$.

The charge-neutral, spherical calcite parcels with a diameter equal 10 nm were constructed using experimentally determined calcite crystal structure by Graf [61]. The spherical particle consists of 8513 Ca^{2+}/CO_3^{2-} pairs. The Mg^{2+}-substituted analogs were prepared by randomly replacing Ca^{2+} by Mg^{2+}. The particles were immersed in a vacuum or in the bulk of water represented by the OPC3 interaction model [62]. We chose the OPC3 water model because it is one of a few models able to reproduce water dielectric properties and realistically model solvation energetics [63]. The simulation cell for hydrated calcite particles contains calcite particle and 75888 water molecules; the total number of atoms in the primary simulation cell is equal to 270229.

We tested two interaction models for the carbonate solid phase: one developed to accurately reproduce carbonate minerals by Raiteri et al. [64] and a simplified force-field developed for carbonate ion by Zarzycki et al. [65]. The new carbonate ion force-field [65] (Table 1) was developed to describe radionuclide complexation by carbonate ions in the clay interlayer. Here, it is used along with the interaction parameters for Mg^{2+} and Ca^{2+} ions taken from Li et al. [66] to gain computational insight into the surface energetics. The modeling using force-field developed by Raiteri et al. [64] was used to compare relative ion-ion binding energies among two interaction models. The simulations were carried using LAMMPS simulation package [67]. The initial configuration was minimized using 10000 steps of gradient descent. Next, it was heated to 298 K using the Langevin thermostat (collision frequency, γ=1 ps^{-1}). To simulate a particle in the vacuum, we used periodic boundary conditions with a particle in the center of a cubic box a few times much larger than the particle. The simulations were carries out in the canonical ensemble. To simulate a particle immersed in water and the bulk water and solid phases, we optimize cell volume by running an additional 10 ns simulations in the isothermal-isobaric ensemble at ambient conditions using Langevin thermostat (collision frequency, γ=2 ps^{-1}) and Berendsen barostat (pressure relaxation time τ = 1 ps). The production simulations were carried for another 50 ns in the isothermal-isobaric ensemble. The last 10 ns was used to extract variation in the configuration energies of carbonate particle and interfacial energies as a function of Mg^{2+} content.

The carbonate/water (γ_{CW}) and carbonate/vacuum (γ_{CV}) interfacial energies were estimated as a difference in the ensemble-averaged configurational energies divided by the surface area [68, 69]:

$$\gamma_{CW} = \frac{E_{cw} - E_w - E_c}{A} \quad \text{and} \quad \gamma_{CV} = \frac{E_{cv} - E_c}{A} \tag{7}$$

where E_i stands for the ensemble-averaged configuration energy of the carbonate particle in the bulk water or vacuum (E_{cw}, E_{cv}) and the bulk carbonate and water phases (E_c, E_w).

The particle surface area and volume contraction caused by the lattice strained introduced by substituting Ca^{2+} by Mg^{2+} are defined as:

$$\Delta A(x) = \frac{A(x=0) - A(x)}{A(x=0)} \quad \text{and} \quad \Delta V(x) = \frac{V(x=0) - V(x)}{V(x=0)} \tag{8}$$

where x is the fraction of Mg in the solid phase $Ca_{1-x}Mg_xCO_3$.

The gain in the interaction energy of carbonate phase due to Mg^{2+} substitutions is calculated as a difference in the ensemble average configuration energy of pure and substituted carbonate phase simulated either as an infinite solid or a finite particle:

$$\Delta E(x) = \frac{\Delta E(x) - \Delta E(x=0)}{N_{pairs}} \tag{9}$$

where N_{pairs} is the number of cation-anion pairs in the particle or primary simulation cell of a periodically replicated solid continuum.

Table 1. Interaction model for carbonate ion taken from Zarzycki et al. [65].

CO_3^{2-}		Lennard-Jones $U(r) = 4\varepsilon\left[\left(\frac{\sigma}{r}\right)^{12} - \left(\frac{\sigma}{r}\right)^{6}\right]$	
Non-bonded interactions	Charge q[e]	σ [nm]	ε [kJ/mol]
C	1.153707	0.339967	0.35982
O	-1.051236	0.295992	0.87864
Bonded interactions			
C-O bond $U(r) = \frac{1}{2}k(r - r_{eq})^2$	r_{eq} =0.13095 nm	k= 533627.36 kJ/mol/nm²	
O-U-O angle $U(\theta) = \frac{1}{2}k(\theta - \theta_{eq})^2$	θ_{eq}= 120	k= 902.9072 kJ/mol/rad²	
improper periodic dihedral O-O-C-O $U(\phi) = k(1 + \cos(n\phi - \phi_{eq}))$	ϕ_{eq}= 180	k =105.0184 kJ/mol n = 2 (multiplicity)	

2. Results and Discussion

One of the significant challenges in studying the kinetics of calcite precipitation is our limited ability to track simultaneously macroscopic changes in the solution composition and microscopic changes in the appearing solid phase. At present, our understanding of precipitation kinetics comes either from the monitoring solution chemistry or from microscopic studies of the growth of individual particles and surfaces. Here, we present experimental data obtained using an electrophoretic measurement of the ζ-potential as a surface probe, with Ca-selective electrode measurements as a solution probe, thus providing simultaneous insight in the evolution of the electrostatic properties of particle surfaces and accompanying changes in the solution composition. In addition, we show a number of rate law fits, molecular dynamics simulations, and SEM and XDR analysis of the final precipitate.

2.1. Link between changes in ζ-potential and precipitate transformation.

In Fig. 1 we show the time-evolution of electrokinetic potential (ζ-potential) during spontaneous unseeded precipitation

experiment from a slightly supersaturated solution ($SI_{calcite}$ ~2 [48]). We observe a rapid change in pH from 5 to 11 after reagents were mixed, followed by a slow decrease to around 10. In the presence of Mg^{2+}, temporal changes in ζ–potential are less pronounced compared with pure calcium carbonate precipitation. Besides, the ζ(time) curve appears to be shifted towards lower absolute values (i.e., less negative) if the Mg^{2+} ions are present. Because the ionic strength of the solution is kept constant by using the background electrolyte, this reduction in ζ-potential must be related to the evolution of particle size [70] and morphology [48] along the precipitation pathway. The absolute value of ζ-potential, which is a measure of suspension-stabilizing repulsive electrical double layer forces, is correlated with polymorph free energy (i.e., |ζ|-vaterite < |ζ|-aragonite < |ζ|-calcite) [30, 31, 48]. The particle growth is also affecting the magnitude of the ζ-potential [70]. Consequently, the evolution of the ζ–potential reflects both particle transformation towards a more stable polymorph phase and an increase in particle size. These two phenomena are intrinsically coupled, which makes their separation nontrivial. In principle, the ζ-potential can be fitted with analytical models that link electrostatics properties with the activities of potential determining ions [48, 71]. However, as recently reported by Heberling et al. [72] it is unclear which ions should be considered as the potential determining ions. For instance, Heberling et al. [72] showed that Cl^- ions, which were believed to be innocent, are controlling the surface and diffuse potential of the calcite/electrolyte solution to a similar extent as Ca^{2+} and CO_3^{2-} ions. Therefore, here we refrain from fitting any analytical models [73] or Surface Complexation Models [72, 74] to the measured ζ-potential, despite the existence of a strong correlation between ζ-potential and activity of free calcium in the solution (see Fig. S4).

2.2. Mg^{2+} preserves spherulitic morphology of magnesium carbonate

The SEM images of particles obtained 2.5 hours after reagents were mixed confirm that Mg^{2+} ions retain spherulitic morphologies (Fig. 2), whereas in the absence of Mg^{2+} we obtain mostly rhombohedral morphologies typical of calcite. Interestingly, the proportion of calcite-like to vaterite-like particles depends on the Mg/Ca ratio. In the case of 1:1 ratio, we obtain a roughly 1:2 ratio of calcite to vaterite, whereas if the initial Mg:Ca rate was 1:1, the majority of particles have spherulitic vaterite-like morphology (Fig. 2).

2.3. Mg^{2+} delays precipitate transformation

We have probed how the electrical double layer developed at the particle/electrolyte interface evolves in time and double-layer forces stabilizes suspensions by analyzing ζ-potential. To quantify growth rates and precipitate composition, we monitor temporal changes in the bulk solution chemistry, namely, the free calcium ion concentration changes, as indicated by the Ca-selective electrode(Figs. 3,4). At the beginning of the precipitation experiment, Na_2CO_3 solution is added to $CaCl_2$, NaCl with/without $MgCl_2$. Despite stirring, supersaturated conditions can be created locally around dropped Na_2CO_3, and some kind of the metastable calcium carbonate phase is formed (e.g., amorphous or vaterite-like phases). This phenomenon is evident from the initial drop in free calcium concentration occurring within ~ a minute after reagents were mixed, followed by increased calcium concentration in the bulk solution (Fig. 3). To set up consistently the starting time for each nucleation experiment, we reset a clock at the moment of time at which calcium free concentration in bulk reaches a minimum after reagents were mixed (illustrated in Figs. 3, S1-S3).

Next, these early precipitate starts to dissolve and transform into vaterite-type intermediate [48]. The peak observed in the free calcium ion concentration in Fig. 4 corresponds to the point in time when dissolution is overcome by the precipitation of a more stable solid phase (see also Figs. S1-S3). This event is delayed by 3 and 6 minutes if Mg^{2+} ions are

present in the initial Mg:Ca ratio equals 1:2 and 1:1, respectively (Fig. 4). Note that time t_0 =0 corresponds to the onset of the nucleation; that is, the induction period and reagent mixing time are not included (Fig. 3). The peak in Fig. 4 has a different origin than peaks in a continuous titration of the carbonate solution with $CaCl_2$ reported by Gebauer et al. [24, 75]. In our study, the peak corresponds to the moment at which dissolution of the intermediate phases is overtaken by the precipitation and growth of a more stable carbonate phase. In contrast, the peak in continuous titration experiments [75] corresponds to the moment at which solution supersaturation is reached, and the carbonate phase precipitation is anticipated.

2.4. Precipitate composition varies in time

The precipitate analysis is based on several assumptions regarding the Mg^{2+} incorporation mechanism. First, we assume that in the solution containing Mg^{2+}, the solid grows by congruently incorporating Mg^{2+} and Ca^{2+} ions. Second, we assume that the amount of Mg^{2+} being incorporated into precipitate can be estimated from the excess of free calcium in the solution in the presence of Mg^{2+} with respect to the Mg-free system (Fig. 5a). Finally, we assume that a similar amount of solid is formed at the same time, and therefore the composition of solid-phase can be estimated using eqs. (3,4). In Fig. 5b,c we show how excess Ca^{2+} in solution, solid composition, and distribution coefficient are changing along the precipitation pathway. The values of distribution coefficient at the end of experiments (D= 0.067 for 1:2 Mg:Ca ratio, and D= 0.025 for 1:1 Mg:Ca ratio) agree well with those reported by Mucci and Morse [6, 9].

The metastable phase formed initially is up to five times enriched in Mg^{2+} as compared with the final precipitate (see Fig. 5b,c). It appears that incorporated Mg^{2+} ions are gradually released to the solution during the transformation from Mg-rich to Mg-poor solid phases. The fraction of Mg^{2+} in the final precipitate (x $Ca_{1-x}Mg_xCO_3$) is equal to 0.13 and 0.146 for the initial Mg:Ca ratio in solution equals 1:2 and 1:1, respectively.

2.5. From changes in solution composition to growth rates

In Fig. 6 we show an estimation of growth/transformation rates obtained from the temporal changes in free calcium concentration in the solution. The rate of transformation (dissolution within the first minutes, followed by growth/transformation at a later time) is the fastest in the case of Mg-free solution – as assessed by comparing curve slopes.

In order to quantify growth inhibition caused by Mg^{2+}, we fitted a few rate law models that have been used previously to model the carbonate precipitation rate (see Supporting Information). The system kinetics is captured by a model assuming dissolution and (re)precipitation operating simultaneously (Fig. 6). The values of the reaction rate constants are consistent with the notion of Mg^{2+} delaying nucleation. It is important to note that kinetic rate laws describe the macroscopic changes in the bulk solution composition, and therefore reflect the effective rate – an average of many co-occurring phenomena. The assumption that nucleation/transformation is dissolution-dominated processes at the beginning, and later it is precipitation-dominated processes is based solely on the experimental data (Figs. 5,6). The transition between these two kinetic regimes occurs at the time corresponding to the peak position (Fig 6). By fitting the macroscopic rate law to experimental data, we confirm that processes occurring before that time are on average captured by the dissolution, and the processes occurring after are on average captured by precipitation.

2.6. Crystal structure

In order to gain insight into crystal structure modification introduced by Mg2+ substitutions into carbonate lattice, we carried out X-ray diffraction measurement of precipitate three hours after reagents were mixed. In Fig. 7a we show the calculated XRD spectra for the reported experimental structures of calcite [61] and magnesium calcite [76]. Because Mg^{2+} ions are smaller than $Ca^{2+,}$ their presence results in peak shifts towards larger angles. In Fig. 7b we show the experimentally determined XRD spectra from our precipitation experiments. In all cases, the solid preserve the calcite lattice structure, but with the subtle peak shifts due to the Mg^{2+}-substitutions.

2.7. Molecular Dynamics Simulations

In order to gain a molecular-level insight into intriguing phenomena of Mg^{2+}-stabilized spherulitic morphology of magnesium calcite, we carry out molecular dynamics simulations. In a direct simulation approach presented here, we are limited in the size of the system that can be realistically model in a fully atomistic approach. We chose 10 nm in diameter spherical particle as a prototype of spherulitic nanoparticles and used it to simulate surface energy as a function of Mg-fraction in the solid phase. In Fig. 8 we show the molecular configuration of the calcite sphere immersed in water obtained after 50 ns simulation time. In Fig. 9, we show the calculated surface energies, relative surface area/volume contraction, and energetic gain due to Mg^{2+} substitutions.

The previously reported atomistic simulations [68] show that the surface energy of water/calcite surfaces is always lower than for the vacuum/calcite surfaces. For example, de Leeuw and Parker [68] estimated the surface energy of hydrated (1014) surface as equal to 0.16 J/m^2 and dry as equal to 0.59 J/m^2. In another simulation study, de Leeuw and Parker [69] showed that the surface energy of (1014) surface of calcite, dolomite, and magnesite increases with the increasing amount of Mg^{2+} in the solid, but the trend is reversed when the surfaces are hydrated. They estimated the surface energy for the hydrated (1014) of calcite and magnesite as equal to 0.16 and 0.02 J/m^2, respectively.

The direct measurement of calcite surface energies gives values between 0.22 and 0.28 J/m^2, with an average among repeated measurements equals 0.23 J/m^2 [77]. The experimental studies that infer surface energies from the nucleation rates or contact angle measurements show a much wider range of surface energies from 0.007 to 0.28 J/m^2 [73, 78, 79]. The low values of γ have been interpreted as evidence of the heterogeneous nucleation (0.007-0.04), whereas the value of 0.12 J/m^2 is expected for homogenous nucleation [73, 78, 79].

Recently, Bruno et al. [80] showed computationally that Mg^{2+} incorporation into the first few layers of calcite crystals always reduces the surface energy. Similarly, Wright et al. [81], using atomistic simulations, showed that magnesite and dolomite have lower surface energies than calcite, consistent with the surface energies of hydrated surfaces calculated by de Leeuw and Parker [68, 69].

Our simulation results (Fig. 9a) confirm that the carbonate/vacuum surface energy is always larger than for the hydrated surfaces. However, we observe that surface energies decrease with the increasing magnesium content for both dry and hydrated particles. The surface energy of the hydrated spherical calcite particle is equal to 0.21 J/m2, which is slightly larger than the value reported for (1014) crystal face by de Leeuw and Parker [68, 69]. Still, it is within the range of experimental values [73, 77-79]. It is important to remember that previous simulation studies consider specific crystal faces (e.g., the most stable and common 1014), whereas here, we model a perfectly spherical particle.

The fact that surface energy decreases with increasing Mg^{2+} content is evidence that Mg^{2+} stabilizes spherulitic

morphology. The exceptionally low surface energy for particles with large Mg^{2+} content indicates that increasing surface area is thermodynamically favorable. From the thermodynamic point of view, the spherical magnesium calcite particles with high Mg^{2+} content are prone to either transform to particles with lower Mg^{2+} fraction or extent surface area. The latter can only be achieved through dissolution and reprecipitation because the solid phase cannot spread as easily as the fluid phase or through in-solid transformation with formation of Mg-depleted core and Mg-enriched and dissolving outerlayer. Our simulation observations provide an intuitive explanation of the evolution of the Mg^{2+} fraction in the solid. Due to the energetically favorable nucleation of solid with a large amount of Mg^{2+}, the initially formed phases are rich in Mg^{2+}. However, the low surface energies for spherical particles trigger transformation to particles with lower Mg^{2+} fraction. The variation in the solution supersaturation is also favoring magnesium-calcite dissolution and reprecipitation of Mg-poor calcite. The solid and interfacial energy dependence on Mg^{2+} content explains why final spherulitic particles have 13-15 % of Mg^{2+}, whereas the intermediate phases can have more than 30-50%. As the particles dissolve and release Mg^{2+}, the surface energy increases, which in turn favors morphology with the lowest surface area to volume ratio – that is a sphere.

The configuration energy per ion pair decreases with increasing Mg^{2+} content (Fig. 9b). Although we consider coprecipitation of the $MgCO_3$ and $CaCO_3$ instead of MgCO3 growth on CaCO3 surface, our simulation results are consistent with those of de Leeuw [82], showing that the growth of $Mg_xCa_{1-x}CO_3$ is exothermic. What is more, the introduction of Mg^{2+} into calcite lattice generates strain that is expected to destabilize lattice and increase particle solubility. However, if we consider the simultaneous incorporation of Ca^{2+} and Mg^{2+} ions and not the growth of $MgCO_3$ on the $CaCO_3$ particle, then lattice strain is uniformly distributed. The lattice can relax, causing the volume/surface area reduction (Fig. 8c,d). This observation is consistent with the strengthening and toughening magnesium calcite nanoprecipitates observed in some biominerals [34-36].

The force-field used in modeling carbonate particles has not been developed to model ion and ion-pair formation in the aqueous phase; therefore, we compare the simulation prediction with another force-field that was created to model the early stages of carbonate nucleation by Raiteri et al. [64]. In Fig. 9b we compare the relative gain in the interaction energy per ion pair for a spherical particle in vacuum using these two force-fields. Both interaction models show a linear decrease in interaction energy per ion pair with increasing Mg content. What is more, we observe a similar volume and surface area contraction upon Mg^{2+} substitution independently of the interaction model. A more detailed simulation study of carbonate diagenetic evolution using Raiteri et al. [64] force-field will be presented soon.

2.8. Spherulites

The spherulitic carbonates have been found in a number of carbonate environments, including soils, lakes, hypersaline or hyperalkaline lagoons [42]. Because spherulites are often associated with hydrated magnesium clays (e.g., stevensite), it has been suggested that a solution supersaturated with respect to magnesium aluminosilicates is required for spherulite formation [42]. However, Mercedez-Martin et al. [42] did not find spherulites in the precipitates formed in the solution saturated with respect to stevensite. The alternative hypothesis suggests that the presence of organic molecules triggers the formation of spherulites [42]. Indeed, a number of studies have shown that the presence of organic matter can facilitate spherulite formation due to either enhancing incorporation of Mg in the calcite structure (e.g., malic, citric, aspartic acids) or increasing local supersaturation through sequestrating and concentrating cations (e.g., alginic acid, polysaccharides, bacterial outer-membrane) [42-45]. The more recent studies have shown that the presence of Mg^{2+} ions [3, 43] or Mg^{2+}/SO_4^{2-} [83] ion pair are the most important requirement for calcite spherulitic growth. Here, we showed that the

presence of Mg^{2+} in either 1:1 or 1:2 ratio with respect to Ca^{2+} ions is sufficient to trigger spherulitic magnesium calcite formation in unseeded precipitation at room temperature, in agreement with the recent study by Tsao et al. [43].

Regarding the mechanism of spherulite formation, a number of pathways have been proposed [43, 45-47]. For example, it has been suggested that phase separation occurs within the particle into Mg-depleted core and Mg-rich shell or Mg-depleted and Mg-rich domains [3, 43, 45-47]. Here, we observe that initially formed precipitates are up to 5 times enriched in Mg^{2+} compared with the final precipitate. By fitting the affinity-based rate law, we identified that the dissolution of Mg-rich carbonate phases dominates initially. However, it rapidly transforms into Mg-depleted phases, releasing Mg^{2+} to the solution and replacing it with Ca^{2+} in the precipitate. Our observations are consistent with the two-step mechanism proposed by Tsao et al. [43], but do not exclude the possibility that dissolution-precipitation and in-solid phase transition/dissolution pathways are operating simultaneously (see Supporting Information).

3. Summary

Most of the sedimentary carbonates deposited in the marine environments are composed of calcium carbonate minerals with a varying amount of incorporated impurities [5] – among which Mg^{2+} ions are the most abundant. However, understanding how interactions of impurities with carbonate and how their incorporation affects sediments behavior remains a challenge. Here, by simultaneously monitoring changes in the electrokinetic potential and concentration of free calcium ions in the bulk solution, we estimate the time-evolution of composition and growth rates in the spontaneous, unseeded nucleation experiments.

We found that the amount of Mg^{2+} incorporated in the precipitate varies widely along the growth/transformation pathway. The initially formed amorphous/metastable phases are about five times enriched in Mg^{2+} as compared with the final magnesium calcite solid.

A combination of two chemical affinity-based rate expressions, the first order for precipitation and the second order for dissolution, can explain particle evolution in the whole time-domain. The extracted rate constant is consistent with the Mg-delayed transformation of unstable polymorphs into magnesium calcite [5, 53], but the spherulitic morphology is preserved. The transformation of Mg^{2+}-rich to Mg^{2+}-poor carbonate phases that preserve spherulitic morphology has been observed before [43], and can be a part of the transformation pathway – dissolution of the Mg^{2+}-rich particle outerlayer and growth of Mg^{2+}-poor core. The solid-phase transformation within the particle interior that results in the formation of the Mg^{2+}-poor core and Mg^{2+}-rich shell [43], with the latter being preferentially dissolved, will still manifest itself as a precipitation-dissolution on the macroscopic scale.

The amount of spherulitic particles correlates with the initial Mg:Ca ratio in solution. For instance, the initial 1:2 Mg:Ca ratio translates to roughly half of the particles having rhombohedral calcite-like morphology and another half showing spherulitic morphology. In the case of 1:1 Mg:Ca ratio in the initial solution, particle morphology is dominated by spherical shape. For comparison, in the same growth conditions from the Mg-free solution, most of the particles have rhombohedral morphology that is characteristic of calcite. These findings agree with the recent reports by Liu et al. [3] and Tsao et al. [43], showing that Mg^{2+} ions trigger the growth of spherulitic calcite.

Molecular dynamics simulations show that the surface energy of spherical particles decreases with increasing Mg^{2+} content. Mg^{2+} stabilizes spherical particle morphology, but a large fraction of Mg in solid results in low surface energy, which in turn triggers shape-preserving transformation to a solid with much lower Mg content. In a case of a spherical nanoparticle with randomly distributed Mg^{2+} and Ca^{2+} ions, the crystal lattice contracts and toughens [34, 35], as evident

from changes in the particle surface area and volume in molecular simulations and shift in the peak position in X-ray diffraction spectra.

Our findings are relevant for a long-standing question of how impurities influence properties of carbonate sediments, how the environmental conditions control growth, polymorphs transformation, solubility, and particle morphology.

Supporting Information

The illustration of the evolution of pH and free calcium concentration in the soltsolution without rescaling time. The plots of ζ-potential against the bulk concentration of free calcium ions with the statistical analysis of correlations factors (Pearson, Spearman, and Kendall). The uncolored SEM images that are presented in Figs. 2,9. Discussion of extension and modification of the affinity-based rate laws and in-solid transition rate law, and illustration of their ability to fit experimental data reported in Fig. 5.

Acknowledgments

M.P., K.K., K.L., W.P., T.B. were supported by NCN Grant Sonata Bis (UMO-2016/22/E/ST4/00446). C.L. and P.Z. were supported by the U.S. Department of Energy (DOE) Chemical Sciences, Geosciences, and Biosciences Division under Contract DE-AC02-05CH11231. The collaboration between Polish Academy of Sciences and Lawrence Berkeley National Laboratory was made possible thanks to NCN Grant Sonata Bis (UMO-2016/22/E/ST4/00446).

Figures

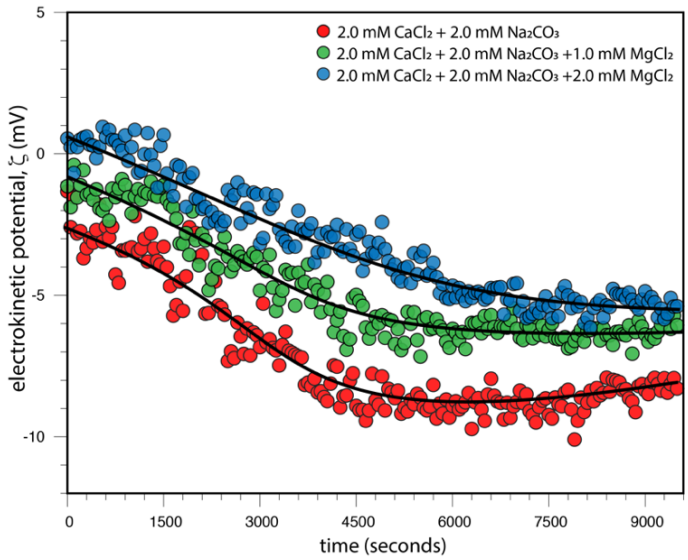

Figure 1. Time evolution of electrokinetic potential measured during spontaneous unseeded precipitation from a slightly supersaturated solution (saturation index with respect to calcite ~ 2[48]) with varying amounts of Mg^{2+} ions. The results for the Mg-free system are taken from Prus et al. [48].

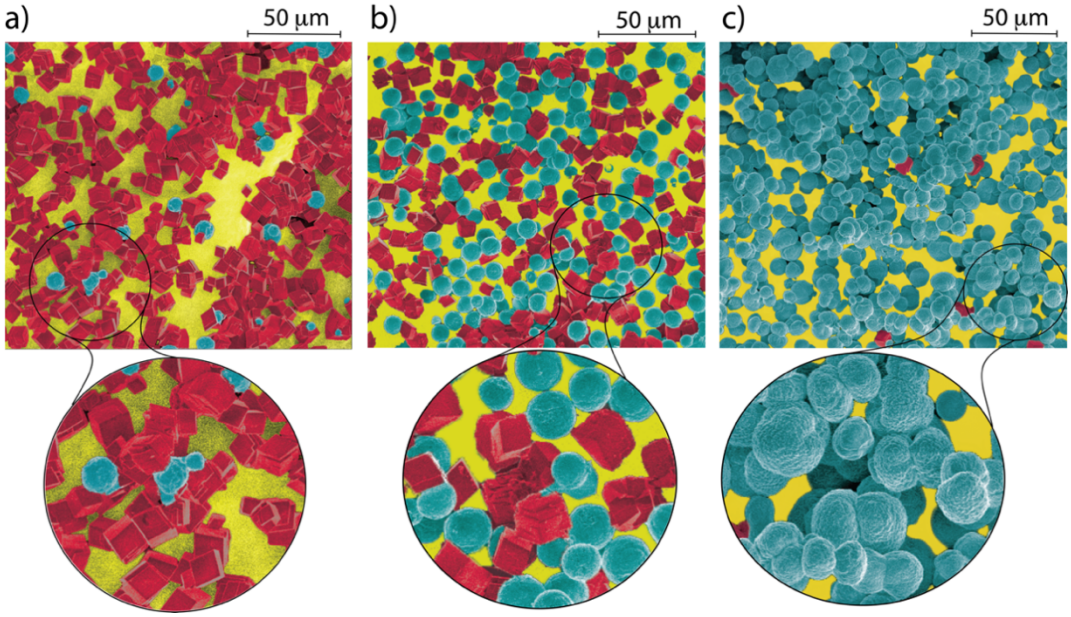

Figure 2. SEM images of calcite and magnesian calcite crystals obtained 2.5 hours after reagents were mixed: a) 2mM $CaCl_2$ + 2mM Na_2CO_3, b) 2mM $CaCl_2$ + 2mM Na_2CO_3 + 1mM $MgCl_2$, c) 2mM $CaCl_2$ + 2mM Na_2CO_3 + 2mM $MgCl_2$. The ionic strength was kept constant by using a background electrolyte (100 mM NaCl). SEM images were colored for reader convenience: the rhombohedral shape is typical of calcite in red and spherulitic morphology characteristic of vaterite in cyan. The presence of Mg^{2+} ions preserves the spherulitic morphology of initially formed metastable vaterite-like phases – similar to the recent study by Liu et al. [3]. The uncolored images are shown in the Supporting Information.

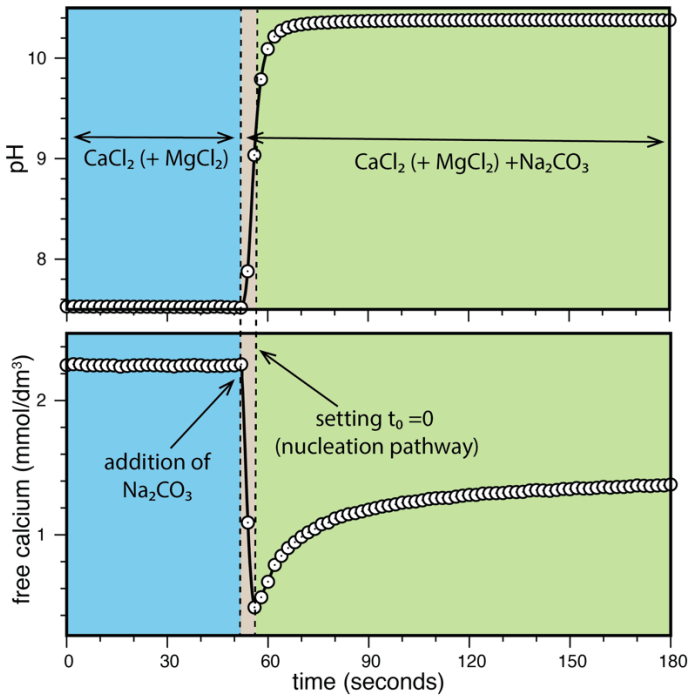

Figure 3. Identification of the carbonate nucleation onset from temporal changes in solution pH (a) and free calcium ions concentration (b) as measured using Ca-ISE and glass electrode. The solution pH and free calcium ions concentration is stable until Na_2CO_3 is added (mixing time, t_{mix}). The calcium concentration drops and pH increases, the time at which the bulk concentration of Ca^{2+} reaches its lowest value is used to restet the time scale (rescale by setting t_0=0). The timescale of the measuremnts shown in Figs. 4-6 are reported with respect to t_0. Here, we show results from one repetition of the precipitation experiments for 2mM $CaCl_2$ + 2mM Na_2CO_3 + 1mM $MgCl_2$.

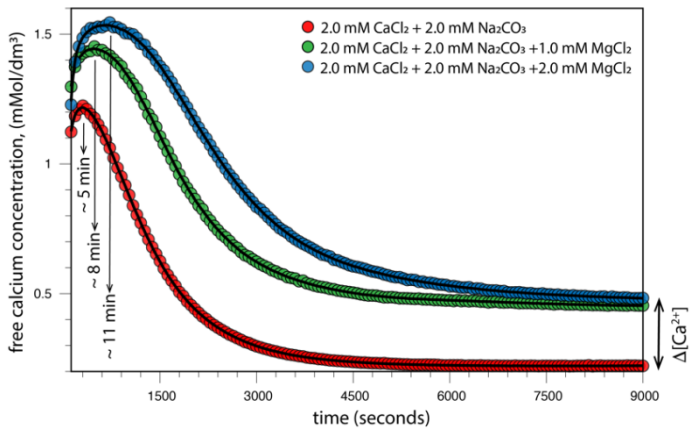

Figure 4. Time evolution of free calcium ions in solution measured using Ca-selective electrode during spontaneous unseeded precipitation from a slightly supersaturated solution (saturation index with respect to calcite ~ 2[48]) with varying amount of Mg^{2+} ions. The results for the Mg-free system are taken from Prus et al. [48].

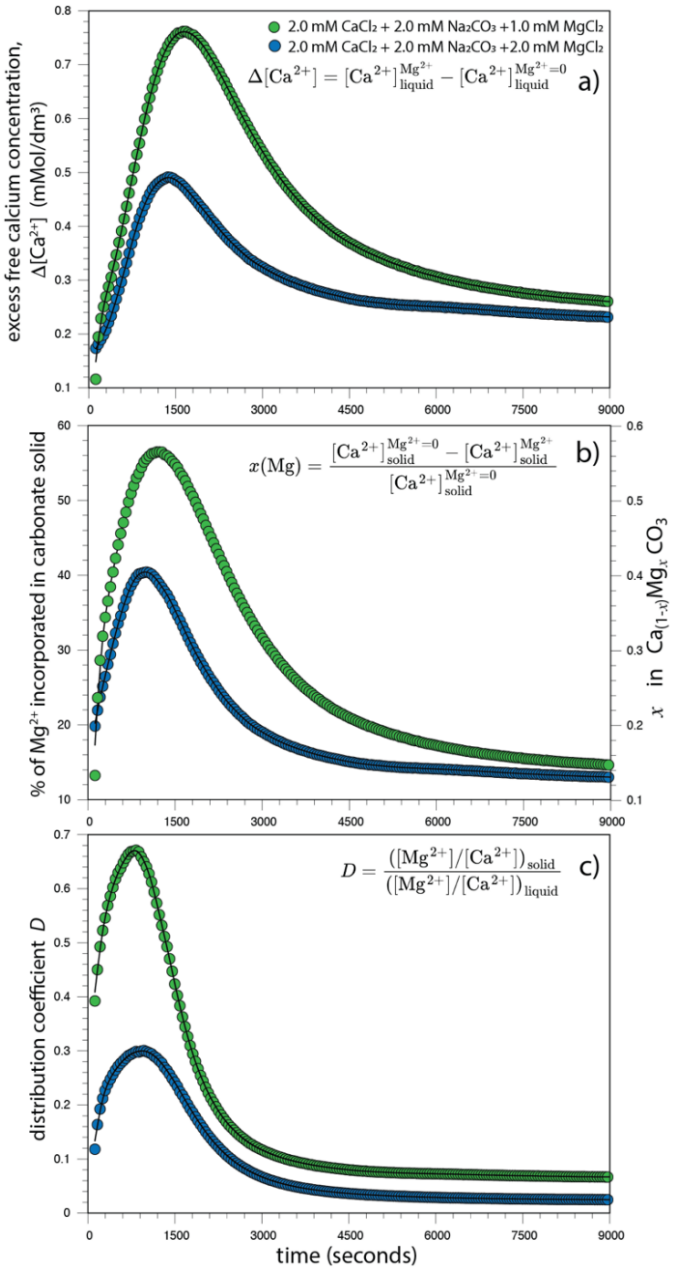

Figure 5. Time-evolution of the excess free calcium in bulk solution in the presence of Mg^{2+} ions (a). The upper bounds for Mg^{2+} incorporation into carbonate precipitate, %, and solid-phase stoichiometry x in $Ca_{1-x}Mg_xCO_3$ (b). The upper-bounds of the Henderson-Kracek distribution coefficient, D (c).

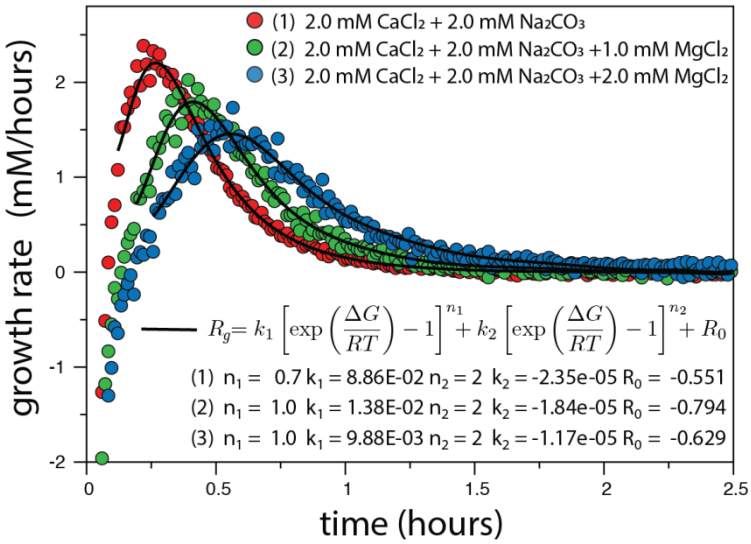

Figure 6. Time-evolution of the carbonate growth rate is estimated from the change in solution composition with time. The fitted analytical model is based on a nonlinear affinity rate law model consisting of simultaneous dissolution of less stable carbonate phase and precipitation of a more stable polymorph. The peak-position defines the crossover of these two kinetic regimes: dissolution- and precipitation-dominated stages. The values of the rate constants (k) for the kinetic model are decreasing with increasing Mg^{2+} concentration. Note that growth rates are not surface-normalized. We introduced a rate shift coefficient, R_0, the best-fit correction factor that accounts for inaccuracy in the calculated saturation state from temporal changes in the bulk calcium composition.

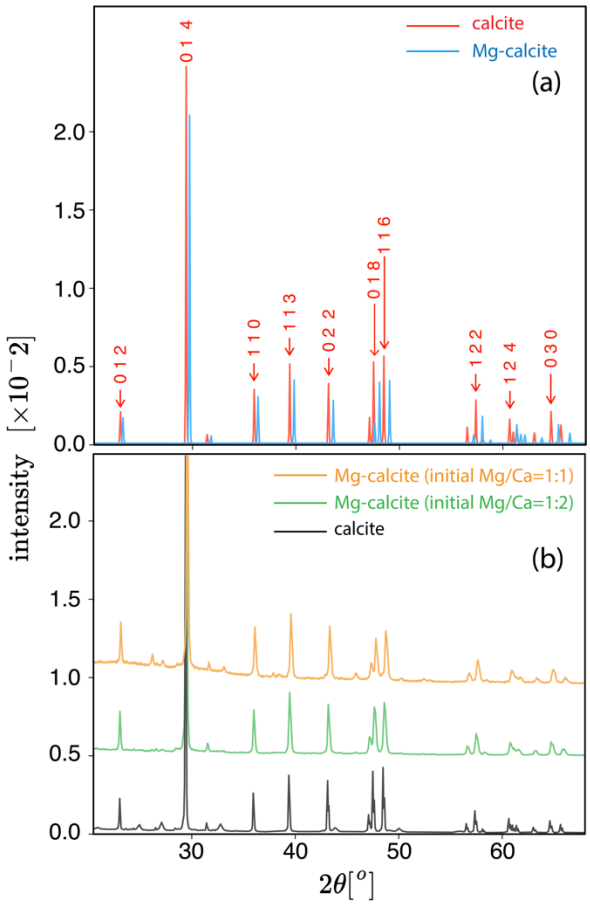

Figure 7. The simulated XRD spectra of the perfect calcite and Mg-calcite structures taken from the literature [61, 76] (a), and experimentally determined XRD spectra for particles obtained in unseeded nucleation experiments three hours after reagents were mixed (b).

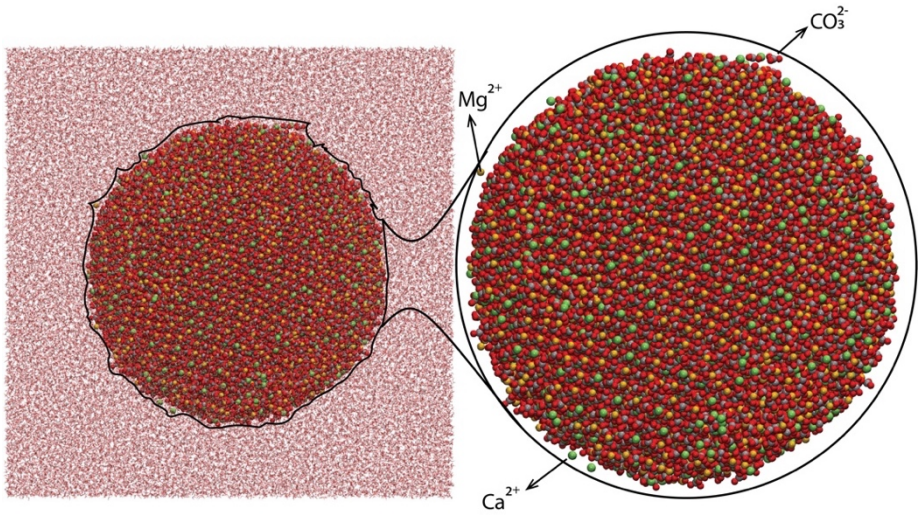

Figure 8. Snapshot of spherical carbonate particle used in the molecular dynamics simulation of bulk and interfacial energies as a function of Mg% content in magnesium calcite. Here, we show the last configuration in 50 ns long simulations of $Mg_{0.7}Ca_{0.3}CO_3$ particle with a final radius equals 4.87 nm. The particle volume contraction is about 18.6% as compared with the unsubstituted carbonate particle.

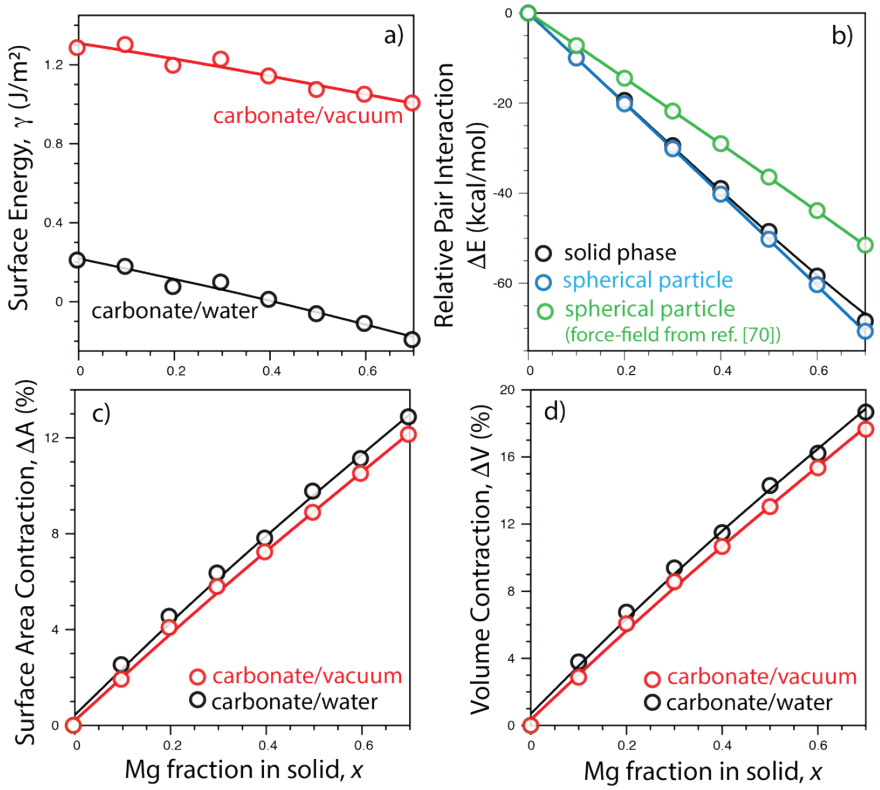

Figure 9. Molecular dynamics simulation of the spherical carbonate particles properties as a function of Mg content: a) surface energy of carbonate/vacuum and carbonate/water interfaces, b) ion-pair interaction energy gain due to Ca^{2+} substitution by Mg^{2+} and crystal lattice contraction in the bulk solid phase and spherical particle, c,d) show a relative contraction of particle surface area and volume as a response to the strain introduced by Ca^{2+} substitution by Mg^{2+}. The simulation carried out using force-field potential developed for carbonate ion by Zarzycki et al. [65], and ion interactions model developed by Li et al. [66] except the relative change in the interaction energy calculated for the spherical particle in vacuum calculated using Raiteri et al. [64] force-field (green circles in panel b).

Table of Contents Graphic

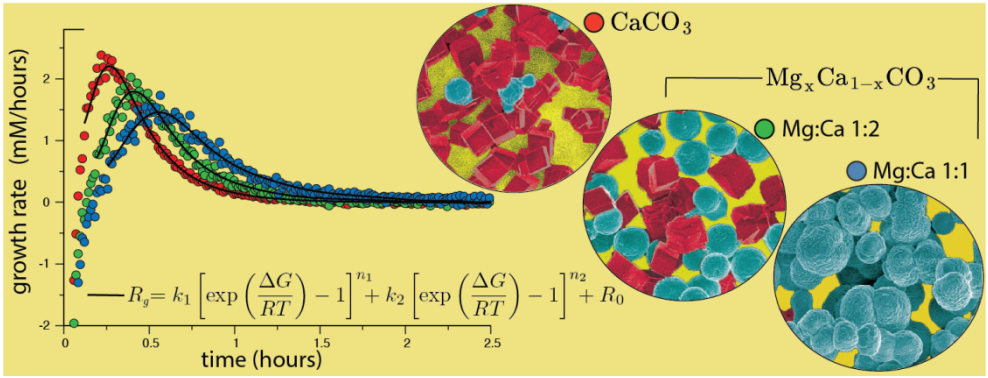

References

[1] K.J. Davis, P.M. Dove, J.J. De Yoreo, The role of Mg2+ as an impurity in calcite growth, Science, 290 (2000) 1134-1137.
[2] J.D. Rimer, Inorganic ions regulate amorphous-to-crystal shape preservation in biomineralization, P Natl Acad Sci USA, 117 (2020) 3360-3362.
[3] Z. Liu, Z. Zhang, Z. Wang, B. Jin, D. Li, J. Tao, R. Tang, J.J. De Yoreo, Shape-preserving amorphous-to-crystalline transformation of CaCO3 revealed by in situ TEM, Proceedings of the National Academy of Sciences, 117 (2020) 3397.
[4] A.E.S. Van Driessche, M. Kellermeier, L.G. Benning, D. Gebauer, New Perspectives on Mineral Nucleation and Growth, in, Springer, Switzerland, 2017.
[5] J.W. Morse, R.S. Arvidson, A. Luttge, Calcium carbonate formation and dissolution, Chemical Reviews, 107 (2007) 342-381.
[6] A. Mucci, J.W. Morse, The Incorporation of Mg2+ and Sr2+ into Calcite Overgrowths - Influences of Growth-Rate and Solution Composition, Geochim Cosmochim Ac, 47 (1983) 217-233.
[7] A. Mucci, J.W. Morse, M.S. Kaminsky, Auger-Spectroscopy Analysis of Magnesian Calcite Overgrowths Precipitated from Seawater and Solutions of Similar Composition, Am J Sci, 285 (1985) 289-305.
[8] A. Mucci, J.W. Morse, Auger-Spectroscopy Determination of the Surface-Most Adsorbed Layer Composition on Aragonite, Calcite, Dolomite, and Magnesite in Synthetic Seawater, Am J Sci, 285 (1985) 306-317.
[9] J.W. Morse, A. Mucci, Composition of Carbonate Overgrowths Produced on Iceland Spar Calcite Crystals Buried in Bahamian Carbonate-Rich Sediments, Sediment Geol, 40 (1984) 287-291.
[10] A. Mucci, J.W. Morse, The Solubility of Calcite in Seawater Solutions of Various Magnesium Concentration, It=0.697-M at 25-Degrees-C and One Atmosphere Total Pressure, Geochim Cosmochim Ac, 48 (1984) 815-822.
[11] J.D. Rodriguez-Blanco, S. Shaw, P. Bots, T. Roncal-Herrero, L.G. Benning, The Role of Mg in the Crystallization of Monohydrocalcite, Geochim. Cosmochim. Acta, 127 (2014) 204-220.
[12] J.D. Rodriguez-Blanco, S. Shaw, P. Bots, T. Roncal-Herrero, L.G. Benning, The Role of pH and Mg on the Stability and Crystallization of Amorphous Calcium Carbonate, J Alloy Compd, 536 (2012) S477-S479.
[13] P. Bots, L.G. Benning, J.D. Rodriguez-Blanco, T. Roncal-Herrero, S. Shaw, Mechanistic Insights into the Crystallization of Amorphous Calcium Carbonate (ACC), Cryst. Growth Des., 12 (2012) 3806-3814.
[14] B. Purgstaller, F. Konrad, M. Dietzel, A. Immenhauser, V. Mavromatis, Control of Mg2+/Ca2+ Activity Ratio on the Formation of Crystalline Carbonate Minerals via an Amorphous Precursor, Cryst. Growth Des., 17 (2017) 1069-1078.
[15] E. Loste, R.M. Wilson, R. Seshadri, F.C. Meldrum, The role of magnesium in stabilising amorphous calcium carbonate and controlling calcite morphologies, J. Cryst. Growth, 254 (2003) 206-218.
[16] J.K. Berg, T. Jordan, Y. Binder, H.G. Borner, D. Gebauer, Mg2+ Tunes the Wettability of Liquid Precursors of CaCO3: Toward Controlling Mineralization Sites in Hybrid Materials, J. Am. Chem. Soc., 135 (2013) 12512-12515.
[17] A. Koishi, A. Fernandez-Martinez, B. Ruta, M. Jimenez-Ruiz, R. Poloni, A. di Tommaso, F. Zontone, G.A. Waychunas, G. Montes-Hernandez, Role of Impurities in the Kinetic Persistence of Amorphous Calcium Carbonate: A Nanoscopic Dynamics View, J Phys Chem C, 122 (2018) 16983-16991.
[18] Z.N. Zhang, Y.D. Xie, X.R. Xu, H.H. Pan, R.K. Tang, Transformation of amorphous calcium carbonate into aragonite, J. Cryst. Growth, 343 (2012) 62-67.
[19] L. Addadi, S. Raz, S. Weiner, Taking Advantage of Disorder: Amorphous Calcium Carbonate and its Roles in Biomineralization, Adv Mater, 15 (2003) 959-970.
[20] M. Alberic, L. Bertinetti, Z.Y. Zou, P. Fratzl, W. Habraken, Y. Politi, The Crystallization of Amorphous Calcium Carbonate is Kinetically Governed by Ion Impurities and Water, Adv Sci, 5 (2018) 1701000(1701001-1701009).
[21] C.R. Blue, A. Giuffre, S. Mergelsberg, N. Han, J.J. De Yoreo, P.M. Dove, Chemical and Physical Controls on the Transformation of Amorphous Calcium Carbonate into Crystalline CaCO3 Polymorphs, Geochim. Cosmochim. Acta, 196 (2017) 179-196.
[22] J.J. De Yoreo, In-Situ Liquid Phase Tem Observations of Nucleation and Growth Processes, Prog Cryst Growth Ch, 62 (2016) 69-88.
[23] J.J. De Yoreo, N.A.J.M. Sommerdijk, Investigating Materials Formation with Liquid-Phase and Cryogenic Tem, Nat Rev Mater, 1 (2016) 1-17.
[24] D. Gebauer, A. Volkel, H. Colfen, Stable Prenucleation Calcium Carbonate Clusters, Science, 322 (2008) 1819-1822.
[25] D. Gebauer, P.N. Gunawidjaja, J.Y.P. Ko, Z. Bacsik, B. Aziz, L.J. Liu, Y.F. Hu, L. Bergstrom, C.W. Tai, T.K. Sham, M. Eden, N. Hedin, Proto-Calcite and Proto-Vaterite in Amorphous Calcium Carbonates, Angew. Chem. Int. Ed., 49 (2010) 8889-8891.
[26] M. Saharay, A.O. Yazaydin, R.J. Kirkpatrick, Dehydration-Induced Amorphous Phases of Calcium Carbonate, J Phys Chem B, 117 (2013) 3328-3336.
[27] J. Ihli, W.C. Wong, E.H. Noel, Y.Y. Kim, A.N. Kulak, H.K. Christenson, M.J. Duer, F.C. Meldrum, Dehydration and Crystallization of Amorphous Calcium Carbonate in Solution and in Air, Nat Commun, 5 (2014) 1-10.

[28] J.W. Singer, A.O. Yazaydin, R.J. Kirkpatrick, G.M. Bowers, Structure and Transformation of Amorphous Calcium Carbonate: A Solid-State Ca-43 NMR and Computational Molecular Dynamics Investigation, Chem Mater, 24 (2012) 1828-1836.
[29] J.M. Walker, B. Marzec, F. Nudelman, Solid-State Transformation of Amorphous Calcium Carbonate to Aragonite Captured by CryoTEM, Angew. Chem. Int. Ed., 56 (2017) 11740-11743.
[30] D. Al Mahrouqi, J. Vinogradov, M.D. Jackson, Zeta Potential of Artificial and Natural Calcite in Aqueous Solution, Adv Colloid Interfac, 240 (2017) 60-76.
[31] I. Sondi, J. Biscan, N. Vdovic, S.D. Skapin, The Electrokinetic Properties of Carbonates in Aqueous Media Revisited, Colloids and Surfaces a-Physicochemical and Engineering Aspects, 342 (2009) 84-91.
[32] M.H. Nielsen, S. Aloni, J.J. De Yoreo, In situ TEM imaging of CaCO3 nucleation reveals coexistence of direct and indirect pathways, Science, 345 (2014) 1158-1162.
[33] L.E. Wasylenki, P.M. Dove, J.J. De Yoreo, Effects of temperature and transport conditions on calcite growth in the presence of Mg2+: Implications for paleothermometry, Geochim Cosmochim Ac, 69 (2005) 4227-4236.
[34] I. Polishchuk, A.A. Bracha, L. Bloch, D. Levy, S. Kozachkevich, Y. Etinger-Geller, Y. Kauffmann, M. Burghammer, C. Giacobbe, J. Villanova, G. Hendler, C.Y. Sun, A.J. Giuffre, M.A. Marcus, L. Kundanati, P. Zaslansky, N.M. Pugno, P.U.P.A. Gilbert, A. Katsman, B. Pokroy, Coherently aligned nanoparticles within a biogenic single crystal: A biological prestressing strategy, Science, 358 (2017) 1294-1298.
[35] D.M. Duffy, Coherent nanoparticles in calcite A toughening strategy known to metallurgists is also used by the brittlestar, Science, 358 (2017) 1254-1255.
[36] A. Broad, I.J. Ford, D.M. Duffy, R. Darkins, Magnesium-rich nanoprecipitates in calcite: atomistic mechanisms responsible for toughening in Ophiocoma wendtii, Phys Chem Chem Phys, 22 (2020) 10056-10062.
[37] R.M. Pytkowicz, Calcium-Carbonate Retention in Supersaturated Seawater, Am J Sci, 273 (1973) 515-522.
[38] F.C. Meldrum, H. Colfen, Controlling Mineral Morphologies and Structures in Biological and Synthetic Systems, Chemical Reviews, 108 (2008) 4332-4432.
[39] F.C. Meldrum, S.T. Hyde, Morphological influence of magnesium and organic additives on the precipitation of calcite, J Cryst Growth, 231 (2001) 544-558.
[40] J.J. De Yoreo, P.U.P.A. Gilbert, N.A.J.M. Sommerdijk, R.L. Penn, S. Whitelam, D. Joester, H.Z. Zhang, J.D. Rimer, A. Navrotsky, J.F. Banfield, A.F. Wallace, F.M. Michel, F.C. Meldrum, H. Colfen, P.M. Dove, Crystallization by particle attachment in synthetic, biogenic, and geologic environments, Science, 349 (2015).
[41] F.C. Meldrum, Calcium carbonate in biomineralisation and biomimetic chemistry, Int Mater Rev, 48 (2003) 187-224.
[42] R. Mercedes-Martin, M.R. Rogerson, A.T. Brasier, H.B. Vonhof, T.J. Prior, S.M. Fellows, J.J.G. Reijmer, I. Billing, H.M. Pedley, Growing spherulitic calcite grains in saline, hyperalkaline lakes: experimental evaluation of the effects of Mg-clays and organic acids, Sediment Geol, 335 (2016) 93-102.
[43] C. Tsao, P.T. Yu, S.L. Li, I.J. Hsu, Y.C. Chuang, C.K. Chang, S.J. Chen, J.C.C. Chan, Ambient Formation of Spherulites of Mg-Calcite in an Aqueous Lipid Solution through the Interplay between Multiple Pathways, J Phys Chem C, 124 (2020) 20538-20546.
[44] A. Sanchez-Navas, A. Martin-Algarra, M.A. Rivadeneyra, S. Melchor, J.D. Martin-Ramos, Crystal-Growth Behavior in Ca-Mg Carbonate Bacterial Spherulites, Cryst Growth Des, 9 (2009) 2690-2699.
[45] C. Zhong, C.C. Chu, On the Origin of Amorphous Cores in Biomimetic CaCO3 Spherulites New Insights into Spherulitic Crystallization, Cryst Growth Des, 10 (2010) 5043-5049.
[46] R. Beck, J.P. Andreassen, The onset of spherulitic growth in crystallization of calcium carbonate, J Cryst Growth, 312 (2010) 2226-2238.
[47] R. Beck, J.P. Andreassen, Spherulitic Growth of Calcium Carbonate, Cryst Growth Des, 10 (2010) 2934-2947.
[48] M. Prus, K. Szymanek, J. Mills, L.N. Lammers, W. Piasecki, K. Kedra-Krolik, P. Zarzycki, Electrophoretic and potentiometric signatures of multistage CaCO3 nucleation, J Colloid Interf Sci, 544 (2019) 249-256.
[49] M.M. Reddy, G.H. Nancollas, Crystallization of Calcium Carbonate .1. Isotopic Exchange and Kintics, J Colloid Interf Sci, 36 (1971) 166-+.
[50] G.H. Nancollas, M.M. Reddy, Crystallization of Calcium Carbonate .2. Calcite Growth Mechanism, J Colloid Interf Sci, 37 (1971) 824-+.
[51] G.H. Nancollas, M.M. Reddy, Kinetics of Crystal Growth from Aqueous Solution, J Electrochem Soc, 118 (1971) C216-+.
[52] L.M. Henderson, F.C. Kracek, The fractional precipitation of barium and radium chromates, J Am Chem Soc, 49 (1927) 738-749.
[53] H.H. Teng, P.M. Dove, J.J. De Yoreo, Kinetics of calcite growth: Surface processes and relationships to macroscopic rate laws, Geochim Cosmochim Ac, 64 (2000) 2255-2266.
[54] A.C. Lasaga, Transition state theory, Reviews in Mineralogy and Geochemistry, 8 (1981) 135-168.
[55] A.C. Lasaga, J.M. Soler, J. Ganor, T.E. Burch, K.L. Nagy, Chemical-Weathering Rate Laws and Global Geochemical Cycles, Geochim Cosmochim Ac, 58 (1994) 2361-2386.
[56] A.C. Lasaga, Kinetic theory in the earth sciences, Princeton University Press, Princeton, 1998.

[57] P. Aagaard, H.C. Helgeson, Thermodynamic and Kinetic Constraints on Reaction-Rates among Minerals and Aqueous-Solutions .1. Theoretical Considerations, Am J Sci, 282 (1982) 237-285.
[58] R. Shiraki, S.L. Brantley, Kinetics of near-Equilibrium Calcite Precipitation at 100-Degrees-C - an Evaluation of Elementary Reaction-Based and Affinity-Based Rate Laws, Geochim Cosmochim Ac, 59 (1995) 1457-1471.
[59] K.L. Nagy, A.C. Lasaga, Dissolution and Precipitation Kinetics of Gibbsite at 80-Degrees-C and Ph-3 - the Dependence on Solution Saturation State, Geochim Cosmochim Ac, 56 (1992) 3093-3111.
[60] K.L. Nagy, A.E. Blum, A.C. Lasaga, Dissolution and Precipitation Kinetics of Kaolinite at 80-Degrees-C and Ph 3 - the Dependence on Solution Saturation State, Am J Sci, 291 (1991) 649-686.
[61] D.L. Graf, Crystallographic Tables for the Rhombohedral Carbonates, Am Mineral, 46 (1961) 1283-1316.
[62] S. Izadi, A.V. Onufriev, Accuracy limit of rigid 3-point water models, J Chem Phys, 145 (2016).
[63] P. Zarzycki, B. Gilbert, Temperature-dependence of the dielectric relaxation of water using non-polarizable water models, Phys Chem Chem Phys, 22 (2020) 1011-1018.
[64] P. Raiteri, R. Demichelis, J.D. Gale, Thermodynamically Consistent Force Field for Molecular Dynamics Simulations of Alkaline-Earth Carbonates and Their Aqueous Speciation, J Phys Chem C, 119 (2015) 24447-24458.
[65] P. Zarzycki, M. Whittaker, L. Zheng, B. Gilbert, Prediction of the Mobility of Uranium(VI) Complexes in Smectite Interlayers, in: ACS Fall 2020 Virtual Meeting & Expo, ACS, San Francisco, 2020.
[66] Z. Li, L.F. Song, P. Li, K.M. Merz, Systematic Parametrization of Divalent Metal Ions for the OPC3, OPC, TIP3P-FB, and TIP4P-FB Water Models, J Chem Theory Comput, 16 (2020) 4429-4442.
[67] S. Plimpton, Fast Parallel Algorithms for Short-Range Molecular-Dynamics, J Comput Phys, 117 (1995) 1-19.
[68] N.H. de Leeuw, S.C. Parker, Surface structure and morphology of calcium carbonate polymorphs calcite, aragonite, and vaterite: An atomistic approach, J Phys Chem B, 102 (1998) 2914-2922.
[69] N.H. de Leeuw, S.C. Parker, Surface-water interactions in the dolomite problem, Phys Chem Chem Phys, 3 (2001) 3217-3221.
[70] K. Kedra-Krolik, K.M. Rosso, P. Zarzycki, Probing size-dependent electrokinetics of hematite aggregates, J Colloid Interf Sci, 488 (2017) 218-224.
[71] P. Zarzycki, P. Szabelski, W. Piasecki, Modelling of zeta-potential of the montmorillonite/electrolyte solution interface, Appl Surf Sci, 253 (2007) 5791-5796.
[72] F. Heberling, T. Klacic, P. Eng, T. Preocanin, J. Lützenkirchen, Structure and Surface Complexation of the Calcite-Water-Interface, in: Goldschmidt 2019, Barcelona, Spain, 2019.
[73] M. Donnet, P. Bowen, J. Lemaitre, A thermodynamic solution model for calcium carbonate: Towards an understanding of multi-equilibria precipitation pathways, J Colloid Interf Sci, 340 (2009) 218-224.
[74] F. Heberling, D. Bosbach, J.D. Eckhardt, U. Fischer, J. Glowacky, M. Haist, U. Kramar, S. Loos, H.S. Muller, T. Neumann, C. Pust, T. Schafer, J. Stelling, M. Ukrainczyk, V. Vinograd, M. Vucak, B. Winkler, Reactivity of the Calcite-Water-Interface, From Molecular Scale Processes to Geochemical Engineering, Appl Geochem, 45 (2014) 158-190.
[75] D. Gebauer, H. Colfen, A. Verch, M. Antonietti, The Multiple Roles of Additives in CaCO3 Crystallization: A Quantitative Case Study, Adv Mater, 21 (2009) 435-439.
[76] P.L. Althoff, Structural Refinements of Dolomite and a Magnesian Calcite and Implications for Dolomite Formation in Marine-Environment, Am Mineral, 62 (1977) 772-783.
[77] J.J. Gilman, Direct Measurements of the Surface Energies of Crystals, J Appl Phys, 31 (1960) 2208-2218.
[78] J. GomezMorales, J. TorrentBurgues, R. Rodriguez-Clemente, Nucleation of calcium carbonate at different initial pH conditions, J Cryst Growth, 169 (1996) 331-338.
[79] O. Sohnel, J.W. Mullin, Precipitation of Calcium-Carbonate, J Cryst Growth, 60 (1982) 239-250.
[80] M. Bruno, E. Bittarello, F.R. Massaro, D. Aquilano, The effect of impurities on the structure and energy of a crystal surface: Mg impurities in calcite as a case study, Crystengcomm, 20 (2018) 4556-4564.
[81] K. Wright, R.T. Cygan, B. Slater, Structure of the (10(1)over-bar4) surfaces of calcite, dolomite and magnesite under wet and dry conditions, Phys Chem Chem Phys, 3 (2001) 839-844.
[82] N.H. de Leeuw, Molecular dynamics simulations of the growth inhibiting effect of Fe2+, Mg2+, Cd2+, and Sr2+ on calcite crystal growth, J Phys Chem B, 106 (2002) 5241-5249.
[83] S.L. Tracy, C.J.P. Francois, H.M. Jennings, The growth of calcite spherulites from solution I. Experimental design techniques, J Cryst Growth, 193 (1998) 374-381.

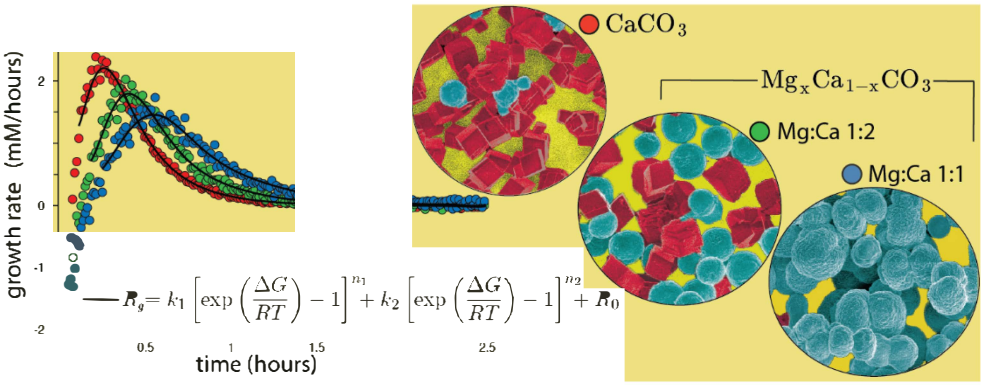
growth rate (mM/hours)
2
0
-1
-2
0.5
1
1.5
2.5
time (hours)
$R_g = k_1\left[\exp\left(\frac{\Delta G}{RT}\right)-1\right]^{n_1} + k_2\left[\exp\left(\frac{\Delta G}{RT}\right)-1\right]^{n_2} + R_0$
$CaCO_3$
$Mg_xCa_{1-x}CO_3$
Mg:Ca 1:2
Mg:Ca 1:1

Marzena Prus: Methodology, Investigation, Writing - Review & Editing, **Chunhui Li:** Validation, Software, Writing - Review & Editing, **Karolina Kedra-Krolik:** Resources, Supervision **Wojciech Piasecki:** Supervision, Resources, Writing - Review & Editing
Karolina Lament: Validation, Writing - Review & Editing **Tajana Begović**: Supervision, Resources **Piotr Zarzycki:** Conceptualization, Methodology, Software, Formal analysis, Visualization, Writing - Original Draft, Writing - Review & Editing, Supervision